Version of Record: https://www.sciencedirect.com/science/article/pii/S0168192320301143
Manuscript_5f6040a6005a9682062699092e58730d

Impacts of spectrally resolved irradiance on photolysis frequency calculations within a forest canopy

Zachary Moon[a], Jose D. Fuentes[a,*], Ralf M. Staebler[b]

[a] *Department of Meteorology and Atmospheric Science, The Pennsylvania State University, University Park, PA, USA*
[b] *Air Quality Research Division, Environment and Climate Change Canada, 4905 Dufferin Street, Toronto, ON, Canada*

Abstract

Although photolysis frequencies are wavelength-dependent and the dependence varies among chemical species, previous canopy radiative transfer models did not consider more than three broad bands (ultraviolet, photosynthetically active radiation (PAR), and near-infrared). In this study, high spectral resolution and wavelength-dependent idealized leaf optical properties allow us to determine the disposition of the light spectrum within a mixed deciduous forest canopy. Four radiative transfer approaches of varying complexity are applied to obtain vertical profiles of spectral actinic flux. Broad-band radiation measurements made above and below a mixed deciduous forest provide the necessary information to verify the fidelity of each radiative transfer approach. Model comparison results indicate that the Beer–Lambert scheme gives less total actinic flux, while the other three schemes give similar actinic flux profiles. Spectral actinic flux profiles are used to calculate in-canopy photolysis for different chemical species and to assess the importance of in-canopy photochemistry in modifying biogenic volatile organic compounds transported to the overlying atmospheric boundary layer. We find that, depending on the time of day and chemical species, percent errors in photolysis frequencies incurred by using a common in-canopy approximation based on weighting by relative PAR profiles can be as high as ±50 % in lower regions of the canopy, or 10–20 % in daily canopy integrated photolysis frequency. Results obtained using a one-dimensional photochemical model suggest that choice of canopy radiative transfer scheme can have substantial impacts on in-canopy chemical reactions and concentrations in the overlying atmospheric boundary layer air. Such effects caused in-canopy gas concentration differences ranging from 8 % for ozone and 35 % for hydroxyl radical to 77 % for nitrate radical.

Keywords: ***photolysis, radiative transfer, actinic light, isoprene, monoterpenes***

*Corresponding author
Email address: jdfuentes@psu.edu (Jose D. Fuentes)

1. Introduction

Plant canopies not only absorb incoming solar irradiance but also modify the quality of the surrounding energy due to the processes of light scattering by foliage elements. Knowledge of light absorption and scattering is crucial to properly quantify plant-atmosphere exchange processes and photochemical reactions within plant canopies. It is not always possible to experimentally determine spectrally resolved irradiance disposition within plant canopies because of the logistics of deploying spectral radiometers at different levels and deriving spatial representations of solar irradiance interception. For tall forests, instantaneous and integrated levels of actinic fluxes need to be determined within canopies to investigate photochemical processes of chemical species amenable to photolysis (Bohn, 2006; Fuentes et al., 2007, 2016). Photochemical processes are key aspects of atmospheric chemistry because photolysis of molecules by actinic irradiance produces reactive free radicals, which largely initiate and enhance the degradation of many trace gases including plant-emitted biogenic volatile organic compounds, BVOCs (Fuentes et al., 2000). Actinic irradiance can also destroy free radicals such as the nitrate radical (NO_3).

Emissions of gases from vegetation and photochemical reactions depend on the wavelength of the light. In forested environments, BVOCs are abundantly produced. Isoprene and members of the terpene family, emitted mostly by trees and flowers, account for more than half of total global BVOC emissions (Guenther et al., 2012). These compounds are oxidized relatively swiftly (with chemical lifetimes on the order of hours to days) by hydroxyl radical (HO), ozone (O_3), and NO_3. Different molecules require actinic light of different wavelengths (λ) to undergo photolysis. For example, different wavelengths of actinic irradiance are required for the photolysis of O_3 and nitrogen dioxide (NO_2) (Bohn, 2006).

$$O_3 + h\nu \longrightarrow O_2 + O(^1D) \qquad 295 < \lambda < 325 \text{ nm} \qquad (1)$$

$$NO_2 + h\nu \longrightarrow NO + O(^3P) \qquad 310 < \lambda < 420 \text{ nm} \qquad (2)$$

Photolysis of NO_2 is an important source of ground-state atomic oxygen ($O(^3P)$) which is the immediate precursor of O_3. In the moist atmosphere, the formation of HO depends on the generated excited oxygen atoms ($O(^1D)$) that combines with water vapor (H_2O).

$$O(^1D) + H_2O \longrightarrow 2\,HO \qquad (3)$$

Oxidation of BVOCs generates high yields of formaldehyde (HCHO), acetaldehyde (CH_3CHO), acetone ($(CH_3)_2CO$ or CH_3COCH_3), and unsaturated aldehydes (RCHO, where R is a hydrocarbon group) (Atkinson, 2000). Yields of HCHO from isoprene oxidation are so high (i.e., > 0.8) that they can be used as a proxy to determine spatial emission rates from forests using passive satellite instruments (Palmer et al., 2003; Millet et al., 2018). The BVOC oxidation products can readily undergo photolysis to generate HO. Furthermore, ozonolysis of terpenes generates high yields of HO, with values reaching up to 0.85 for the species with the highest O_3 reactivity (Paulson and Orlando, 1996; Aschmann et al., 2002). In summary, chemical processing of BVOCs in plant canopies can occur during sunlit and dark conditions and generate sufficient free radicals to drive chemical cycles. In addition to the photochemical processes impacting HO concentrations, terpene oxidation produces oxygenated VOCs (OVOCs) capable of partitioning from the gas to the condensed phase and modifying existing aerosol particles or forming new secondary organic aerosols (SOA). Numerous studies have examined these processes for isoprene (e.g., Carlton et al., 2009; Pandis et al., 1991; Kroll and Seinfeld, 2008; O'Halloran et al., 2009; Doughty, 2014) and terpenes (e.g., Barthelmie and Pryor, 1999).

The extent of in-canopy photochemical processing of BVOCs depends on both the level and the spectral distribution of actinic flux. Fluxes of BVOCs from the canopy to the regional atmospheric boundary layer depend on in-canopy oxidant levels (HO formation via photolysis reactions and terpene oxidation, and O_3 and NO_3 concentrations within plant canopies). Air parcel residence times also influence the fraction of BVOCs locally destroyed within the plant canopy (Gerken et al., 2017). For tall forests, in-canopy chemical processing of terpenes can account for more than 10 % of destruction for locally produced gases (e.g., Makar et al., 1999; Stroud et al., 2005; Forkel et al., 2006; Fuentes et al., 2007; Saylor, 2013; Ashworth et al., 2015). Compared to emissions or above-canopy fluxes of isoprene and monoterpenes, the chemical processing is generally of minor magnitude. For some reactive sesquiterpenes such as β-caryophyllene, in-canopy chemical reactions can consume up to 75 % of the locally emitted gases (Strong et al., 2004; Stroud et al., 2005; Rinne et al., 2012), mostly due to ozonolysis. The reported estimates of chemical processing in plant canopies were done with photochemical models that computed the photolysis reactions based on broad-band irradiance (e.g., photosynthetically active radiation (PAR)) estimates, often employing the Beer–Lambert law (e.g., Fuentes et al., 2007). As molecular photolysis rate coefficients (J values, also known as photolysis frequencies) depend on spectrally resolved absorption cross section ($\sigma(\lambda)$), quantum yield ($\phi(\lambda)$), and actinic irradiance flux density ($F(\lambda)$, hereafter referred to as

spectral actinic flux), it is necessary to determine the variations of these quantities as a function of canopy depth and time of day.

Given the importance of chemical processing of reactive gases in forested ecosystems and the dearth of examinations of spectral irradiance transfer and disposition within plant canopies, the goals of this manuscript are fourfold. First, results from field radiative studies are presented and interpreted to estimate seasonal patterns in solar irradiance attenuation by a temperate deciduous forest. Particular emphasis is placed on field studies that were carried out during the leaf senescence period to quantify the degree of light attenuation in response to changes in foliage optical properties (Figure 1). Seasonal investigations to quantify light attenuation by plant canopies are rare. Therefore, this manuscript also reports a unique data set to evaluate radiative transfer models. Second, field measurements are integrated with radiative transfer models to evaluate the most reliable methods of determining radiative transfer in deciduous forests. There is a scarcity of radiative transfer model verification under different leaf optical properties and varying levels of diffuse light. The evaluated radiative transfer models include the Beer–Lambert law, the two-stream approximation (Dickinson, 1983; Sellers, 1985), the four-stream approximation (Tian et al., 2007), and a multiple scattering model (Zhao and Qualls, 2005). Third, a spectrally resolved radiative transfer method is proposed to determine the spectral actinic flux as a function of canopy depth and applied to calculate in-canopy photolysis frequency profiles. Finally, results are included in a one-dimensional photochemical model to ascertain the nominal uncertainties associated with the estimates of photolysis for molecules amenable to photodissociation in plant canopies.

2. Methods

2.1. Field measurements

Relevant data are available from a 1995 field campaign that took place during 1 June (day of year, DOY 152) to 7 October (DOY 280) at the Borden Forest Research Station (site location 44.317 °N, 79.933 °W) (Staebler et al., 1997) and include: total direct and diffuse solar (wavelengths ranging from 0.3 to 5 µm, model SPP, The Eppley Laboratory, Inc., Newport, RI) irradiance, incoming and reflected PAR (0.4–0.7 µm, model LI190SA, Licor Inc., Lincoln, NB), and net radiation (0.3–80 µm, model CN1-R, Middleton, Australia). Instruments were mounted on a tower above the canopy. Measurements below the canopy were made from a trolley (Figure 1a) while moving at 0.02 $\mathrm{m\,s^{-1}}$ over a transect of 30 m long and were acquired at the frequency of 2 Hz. Such a technique, combined with time averaging, was employed to provide a spatially representative average. This is important

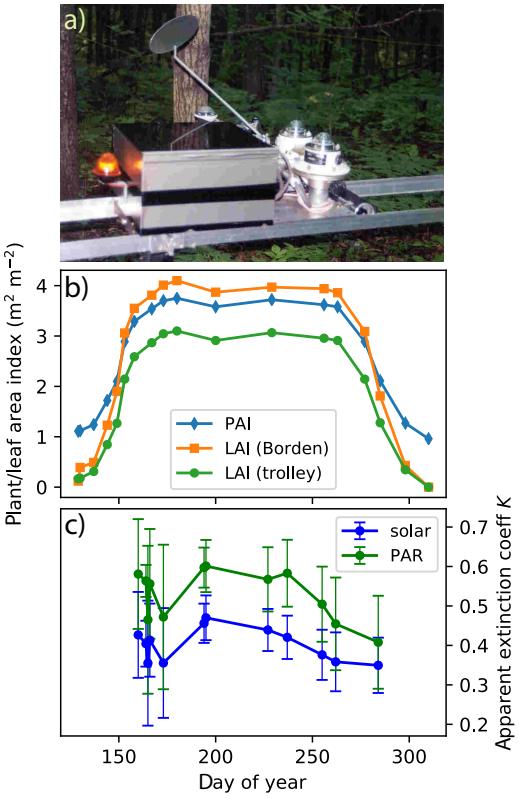

Figure 1: a) Photograph of the instrumented trolley for determining diffuse and direct PAR and solar radiation beneath the canopy; b) LAI seasonality at the trolley site and on average (for ten sites) in the tower surrounding area, and PAI in the tower surrounding area; c) the apparent extinction coefficient for PAR and total solar, calculated from the above and below canopy irradiance measurements and total LAI (L_{tot}), i.e., $I_{below} = I_{above}e^{-KL_{tot}}$. Error bars denote the standard deviation for that day of measurements.

because all of the canopy radiative transfer schemes employed in this study assume a horizontally homogeneous canopy. Staebler et al. (2000) and Teklemariam et al. (2009) described the site in more detail, along with some climatology.

Other measurements included canopy structure variables such as canopy height, seasonal plant area index (PAI) and leaf area index (LAI, Figure 1b) at the trolley site and ten sites within the turbulent energy flux footprint of the tower (Staebler et al., 1997), heights of maximum LAI, height of the upper leaf canopy lower boundary, total LAI in the upper leaf canopy, mean leaf angle, clumping index, etc. The leaf area profile used in the models is derived from these variables. Seasonal variations of extinction coefficients for incoming solar irradiance and PAR are included (Figure 1c) to illustrate the influences of foliage phenology, including senescence, on light transfer in the forest canopy.

Due to logistical challenges, *spectral actinic flux* data in plant canopies are rare (see Bohn, 2006; Bohn et al., 2008). Instead, *broadband irradiance* measurements are more commonly made, which is the case with the measurements used in this study. However, for clear-sky conditions, atmospheric radiative transfer models (e.g., Madronich, 1987; Liou, 2002) are adept at predicting the spectral irradiance reaching the air layer just above the canopy. Combining the output of such models with the above-canopy broadband irradiance measurements, we can estimate the top-of-canopy spectral irradiance. Then, using spectrally resolved leaf optical properties, the disposition of the actinic flux within the canopy can be predicted from measurements at the top of the canopy, provided that information of the spatial distribution and qualities of the foliage elements are known (i.e., LAI as a function of canopy depth, the foliage orientation function $G(\psi)$, etc.). The following sections describe how we obtain each of these required components for this study.

2.2. Leaf optical properties

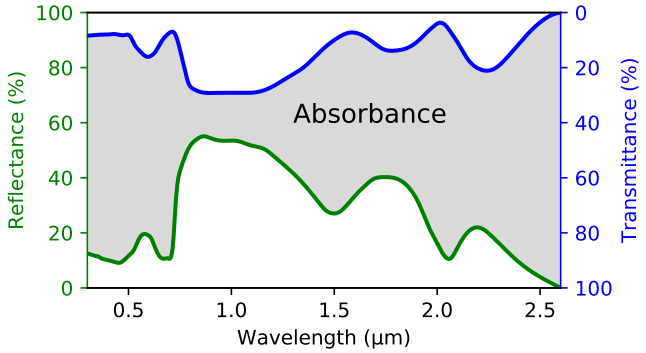

Figure 2: Idealized green leaf reflectance and transmittance, based on Monteith and Unsworth (2013) Figure 6.5. Note that the transmittance is measured from the top, so that the region between the two curves represents absorbance. The optical properties presented here span wavelengths 0.3–2.6 μm.

Figure 2 shows leaf reflectance and transmittance as a function of wavelength. This plot was created by digitizing Figure 6.5 of Monteith and Unsworth (2013), which describes the curves as idealized. Using linear extrapolation, the reflectance and transmittance were extended from 0.35 μm down to 0.30 μm. Figure 2 illustrates that the leaf absorbs strongly in the visible region. Due to the local maximum in reflectance around 0.55 μm, one can deduce that this is a green leaf. Spectral reflectance and transmittance of leaves change throughout the course of the growing season and more significantly during the senescence period (Figure 1c).

2.3. Canopy radiative transfer models

Previous studies investigated the disposition of different wavelength bands in forest canopies, but mostly for PAR, ultraviolet (UV), and near-infrared (N-IR). For example, Fuentes et al. (2007) considered the PAR band only, using a Beer–Lambert-type approach to determine the PAR profile from measurements above and below the canopy. Baldocchi et al. (1984) examined UV, PAR, and N-IR in a deciduous forest using measurements and Beer–Lambert models. Using the PAR profile and J values above the canopy, J values within the canopy can be estimated by using the relative PAR profile to scale them. This approach was considered in Stroud et al. (2005); Fuentes et al. (2007) and many 1-D canopy modeling studies (e.g., Forkel et al., 2006; Ashworth et al., 2015; Saylor, 2013). Stroud et al. (2005) calculated isoprene and monoterpene (α-pinene and β-pinene) processing within a pine-sweetgum forest canopy to be less than 10 % of the emissions within the canopy. Notably, Bohn (2006) made measurements of spectral actinic flux above and within a forest canopy at a tower site, and calculated isoprene and monoterpene processing to be less than 4 %, consistent with the results of Stroud et al. (2005). However, Stroud et al. (2005) also calculated that the chemical processing of β-caryophyllene, a prominent sesquiterpene, can be as high as 75 % due to mostly ozonolysis. Furthermore, it is important to recognize that these chemical processing calculations are sensitive to assumptions about air parcel residence times (Gerken et al., 2017) and the turbulent transport characteristics within the canopy.

Comparisons of canopy radiative transfer schemes used by the forest gas-exchange/photochemistry (1-D modeling) and Earth system modeling communities are rare (exceptions include Wang (2003) and Yuan et al. (2017)). Wang (2003) compared three canopy radiative transfer schemes: a Beer–Lambert-based formulation, that of Goudriaan (1977), and the two-stream scheme of Sellers (1985). The Beer–Lambert method was found to systematically overestimate light absorption, up to 50 % in the N-IR band when compared to the other two methods. Compared to the two-stream, the Goudriaan method gave significantly less absorbed visible diffuse radiation for low values of LAI (< 2.5). Yuan et al. (2017) tested a modified two-stream model in the context of the Community Land Model (CLM4.5). In the vegetation (satellite) remote sensing community, controlled, in-depth comparisons are conducted (e.g., the Radiative Transfer Model Intercomparison (RAMI) projects: Widlowski et al., 2007, 2015), and Kuusk (2018) provides an overview of the different types of models.

In the present study, four different 1-D canopy radiative transfer models with varying levels of complexity are compared: the Beer–Lambert (Monteith and Unsworth, 2013; Campbell and Nor-

man, 2012), the two-stream (Dickinson, 1983; Sellers, 1985), the four-stream (Tian et al., 2007), and the multiple scattering (Zhao and Qualls, 2005) models. All models are based upon the horizontally homogeneous turbid medium assumption from radiative transfer theory. In this investigation, we attempt to improve the Beer–Lambert model's prediction of actinic flux by adding a term that approximates the contribution to diffuse light by scattering of the direct beam (described in Section 2.3.1). To get profiles of "spectral" radiation variables, we divide the spectrum into a number of smaller bands and apply the radiative transfer approach to each band individually. This approach is accurate as long as processes that shift frequency such as Raman scattering are negligible. For the sake of completeness, principal features of the radiative transfer models employed in the current study are provided below.

2.3.1. Beer–Lambert model

The Beer–Lambert law is based on the principle of exponential extinction by a homogeneous partially absorbing medium. Light absorption in a leafy model layer depends on the leaf density and distribution, and the following equation describes the light extinction by leaves

$$I(z) = I(h_c)\,\exp\left[-\Omega\frac{G}{\cos(\psi)}L(z)\right] \tag{4}$$

where $I(h_c)$ is the irradiance at the top of the canopy (h_c), $G = G(\psi)$ is the leaf orientation function, Ω is the leaf clumping factor, ψ is the solar zenith angle, and $L(z)$ is the cumulative leaf area index (LAI), accumulating from h_c. The black-leaf extinction coefficient is defined as $K_b(\psi) = G(\psi)/cos(\psi)$. Extinction of the diffuse beam within the canopy is modeled using the diffuse bulk transmissivity

$$\tau_d = 2\int_0^{\pi/2} \tau_b(\psi, L)\sin(\psi)\cos(\psi)\,\mathrm{d}\psi \tag{5}$$

where $\tau_b(\psi, L) = e^{-K_b(\psi)L}$ is the black-leaf transmissivity for the direct beam, i.e., the probability that the direct beam will penetrate to LAI depth without encountering a leaf. However, the Beer–Lambert scheme for canopy radiative transfer as described in Campbell and Norman (2012) does not include a term for conversion of scattered direct to diffuse light (i.e., the leaves are 'black'). An extinction coefficient for 'grey' leaves can be calculated, and is related to that for black leaves ($K_b(\psi)$)

$$K(\psi) = K_b\,(\psi)k' \tag{6}$$

where $k' = \alpha^{0.5}$ is the bulk attenuation coefficient (Monteith and Unsworth, 2013, p. 48). The absorbance α is equal (by Kirchoff's law of thermal radiation) to $1 - \rho - \tau$ where ρ is reflectivity

and τ is transmissivity. Then, we can estimate the term that represents the contribution to diffuse by scattering of the direct beam as

$$I_{b\to d}(L) = I_b(L=0) \cdot \left[e^{-K(\psi)\,L} - e^{-K_b(\psi)\,L}\right] \tag{7}$$

where I_b (the direct beam), $K(\psi)$, and $K_b(\psi)$ depend on wavelength.

2.3.2. Two-stream model

In canopy radiative transfer models employing the two-stream approximation, light is partitioned into two streams: an upward-going stream and a downward-going stream. Light in each stream is separated into direct and diffuse portions to enable a more accurate representation of light scattering processes. Sellers (1985) describes the model and its equations in depth and provides the analytical direct and diffuse irradiance solutions as well. This scheme (Dickinson, 1983; Sellers, 1985) remains the most widely used in regional and climate models that incorporate canopy radiative transfer (Yuan et al., 2017). The following equations make up the model (Sellers, 1985):

$$-\bar{\mu}\frac{\mathrm{d}I\uparrow}{\mathrm{d}L} + [1-(1-\beta)\omega]\,I\uparrow - \omega\beta I\downarrow = \omega\bar{\mu}K\beta_0\exp(-KL) \tag{8}$$

$$\bar{\mu}\frac{\mathrm{d}I\downarrow}{\mathrm{d}L} + [1-(1-\beta)\omega]\,I\downarrow - \omega\beta I\uparrow = \omega\bar{\mu}K(1-\beta_0)\exp(-KL)\ . \tag{9}$$

$I\uparrow$ and $I\downarrow$ represent upward and downward diffuse irradiance streams, respectively, normalized to the irradiance incident above the canopy ($I\downarrow(h_c)$)). The variable $\bar{\mu}$ is the average inverse diffuse optical depth per unit leaf area, calculated as $\int_0^1 \frac{\mu'}{G(\mu')}\,\mathrm{d}\mu'$, where μ' is the cosine of the direction of the scattered flux and G is the foliage orientation function. The cosine of the zenith angle of the incident solar beam is denoted by μ. The scattering coefficient ω is the sum of the leaf-element reflectance α and transmittance τ, i.e., $\omega = \alpha + \tau$. β and β_0 are the diffuse and direct beam upscatter variables, respectively, and K is the extinction coefficient due to light interactions with leaf elements, given by $K = \frac{G(\mu)}{\mu}$, also known as the optical depth of the direct beam per unit leaf area. The K is equivalent to K_b of Section 2.3.1. The terms in Eqs. 8 and 9 are each associated with a relevant physical process. For example, in Eq. 8 the left-hand-side terms represent: (1) attenuation of the upward diffuse, (2) a rescattering upward after interaction with leaf elements, and (3) downward diffuse that is backscattered (i.e., converted to upward diffuse). The right-hand-side term represents the portion of the direct incident flux at depth L that is converted to diffuse and scattered in the upward direction.

2.3.3. Four-stream model

The concepts and basic approach are essentially identical to those in the two-stream model described above. However, instead of one upward and one downward diffuse stream, there are two of each. The version used in this study is from Tian et al. (2007), who based their derivation on Li and Dobbie (1998), adding specific features for vegetative canopies. Tian et al. (2007) reported the four-stream scheme to perform approximately twice as well as a two-stream scheme for low solar elevation angles, using the successive orders of scattering approximation (SOSA) scheme (Myneni et al., 1987) as the reference model. With the four-stream scheme, the zenith space is separated into four regions: $[-1, -\mu_s]$, $[-\mu_s, 0]$, $[0, \mu_s]$, and $[\mu_s, 1]$, where $\mu_s \equiv \cos\theta_s$, and θ_s is the zenith angle separating a hemisphere into two portions or sectors (Li and Dobbie, 1998). Following the suggestion of Tian et al. (2007), we use $\mu_s = 0.501$ (equivalent to $\theta_s = 60°$). This choice of μ_s allows greater solar zenith angles, where the radiation field changes more rapidly, to be solved more accurately.

Thus, for example, the equation for downward diffuse in sector 2 is

$$\frac{\mathrm{d}I{\downarrow_2}}{\mathrm{d}L} = \frac{1}{\mu_2}\left[\left(\alpha^+ - \kappa_{-2}\right) I{\downarrow_2} + \beta^+ I{\downarrow_1} + \beta^- I{\uparrow_1} + \alpha^- I{\uparrow_2}\right] + \frac{G(\mu_0)}{\mu_2}\varepsilon_{-2}\exp\left(\frac{-G(\mu_0)L}{\mu_0}\right) \tag{10}$$

where $\mu_2 = \int_{\mu_s}^{1} \mu\,\mathrm{d}\mu$ defines the sector and the $\alpha^{\pm}$, κ, $\beta^{\pm}$ are various sector integrals of $G(\mu)$ and $P(\mu, \mu')$ (the normalized azimuthally independent phase function; $P(-\mu, \mu') = P(\mu, \mu')$, and $1 = \frac{1}{2}\int_{-1}^{1} P(\mu, \mu')\,\mathrm{d}\mu$; see equations 3a-4g in Tian et al. (2007) for the full set of sectors). After finding the upward and downward stream solutions for isotropic irradiances in each of the sectors, they are combined to give the hemispherical irradiances.

$$I{\uparrow} = 2\pi\left(\mu_1 I{\uparrow_1} + \mu_2 I{\uparrow_2}\right) \tag{11}$$

$$I{\downarrow} = 2\pi\left(\mu_1 I{\downarrow_1} + \mu_2 I{\downarrow_2}\right) \tag{12}$$

In previous applications (Tian et al., 2007), the spherical leaf angle distribution $G(\psi) = 0.5$ was used to simplify the problem whereas in the current implementation the general form of $G(\psi)$ was adopted and the system of equations was solved numerically.

2.3.4. Multi-scattering model

This model is based on the representation of all possible light scattering events that can occur between two layers i and $i+1$ as an infinite series. For example, the total downward hemispherical solar irradiance from vegetation layer $i+1$ to layer i can be expressed as a recursive expression

that converges to

$$SWd_{i+1} = \frac{SWd0_{i+1}}{1 - r_i r_{i+1}(1-\alpha_i)(1-\tau_i)(1-\alpha_{i+1})(1-\tau_{i+1})} + \frac{r_{i+1}(1-\alpha_{i+1})(1-\tau_i)SWu0_i}{1 - r_i r_{i+1}(1-\alpha_i)(1-\tau_i)(1-\alpha_{i+1})(1-\tau_{i+1})}. \quad (13)$$

The $SWd0_{i+1}$ is the downward hemispherical irradiance from vegetation layer $i+1$ to layer i (before taking the multiple scatterings between layers i and $i+1$ into account) and $SWu0_i$ is the the original hemispherical upward irradiance from vegetation layer i to layer $i+1$. Each canopy layer has a fraction (τ_i) of hemispherical irradiance transmitted to layer i without being intercepted by any leaf. The absorptivity (α_i) is the fraction of absorbed to total intercepted irradiance within layer i. The r_i represents backward scattering. The light multi-scattering scheme takes a two-pass approach to calculate canopy irradiance profiles. The first pass encompasses only single scattering processes. The captured processes (radiation penetration through gaps between leaves, and absorption, reflection, and transmission within leafy model layers) are essentially the same as the isosector approaches (two- and four-stream). The primary advantage of this model is its ability to approximately capture the effect of within-layer multiple scattering processes without requiring many iterations (unlike more rigorous solution methods such as Monte Carlo or SOSA mentioned in 2.3.3). Due to the manner that scattering within canopy layers is modeled, results from this approach are sensitive to the number of canopy layers. Zhao and Qualls (2005) suggest > 50 layers be used. In the current study, 60 canopy layers are included.

2.4. Spectral irradiance estimation

Numerous models exist to predict the incoming spectral solar irradiance reaching the top of the canopy. One example is the Bird and Riordan's Simple Spectral Model (SPCTRAL2), which uses surface albedo, aerosol optical depth, atmospheric turbidity, total column ozone, and precipitable water to predict the spectral irradiance at a certain location and time (Bird, 1984; Bird and Riordan, 1986). For clear sky conditions, in the current study we used default transmissivity (tau500 = 0.27) and water vapor path length (watvap = 1.42) quantities, which are reasonable for mid-latitude summer values, and the climatology based calculation of total column ozone included in SPCTRAL2 (Van Heuklon, 1979). Total (wavelength-integrated, direct + diffuse) irradiances for the generated SPCTRAL2 spectra were normalized to the above-canopy irradiance measurements to enable fair comparisons of modeled and measured below-canopy radiation. A correction factor for PAR region bands was constructed as

$$c_{\mathrm{PAR}} = \frac{I_{\mathrm{PAR,meas}}}{\int_{0.4}^{0.7} I_{\mathrm{sp2}}\,\mathrm{d}\lambda}. \quad (14)$$

Here, $I_{\mathrm{sp2}} = I_{\mathrm{sp2}}(\lambda)$ is the spectral irradiance (W m^{-2} µm^{-1}) predicted by SPCTRAL2. The integral is evaluated as a discrete sum over the SPCTRAL2 irradiance (direct + diffuse; W m^{-2}) in PAR bands. The correction factor for the remaining bands of the light spectrum is derived from the difference between the measured total solar and PAR. Ideally, it would be necessary to use measured UV and N-IR irradiance measurements to correct these regions separately, but these measurements were not available.

$$c_{\text{N-IR,UV}} = \frac{I_{\text{tot,meas}} - I_{\text{PAR,meas}}}{\int_{0.3}^{0.4} I_{\mathrm{sp2}}\,\mathrm{d}\lambda + \int_{0.7}^{2.6} I_{\mathrm{sp2}}\,\mathrm{d}\lambda} \tag{15}$$

These correction factors are applied to the initial spectrum I_{sp2} to give the corrected spectrum (I'_{sp2}):

$$I'_{\mathrm{sp2}} = \begin{cases} c_{\mathrm{PAR}} I_{\mathrm{sp2}} & \lambda \in [0.4, 0.7)\ \text{µm} \\ c_{\text{N-IR,UV}} I_{\mathrm{sp2}} & \lambda \notin [0.4, 0.7)\ \text{µm}\ . \end{cases} \tag{16}$$

After these two corrections, the total (direct + diffuse) irradiances in both PAR and total solar regions are consistent with the observations. Of the 122 SPCTRAL2 bands, 108 overlap with the leaf property spectral data; only these are considered in the canopy radiative transfer calculations.

2.4.1. Approximating spectral modification due to cloudiness

Absorption and scattering by cloud particles strongly depend on light wavelength. For example, we should in general expect to obtain higher diffuse IR (due to strong liquid water absorption/emission) at the surface with an overcast cloud layer. SPCTRAL2 is for clear-sky, but it does account for the influence of water vapor. With clouds in the atmospheric column, total precipitable water vapor is typically enhanced by some fraction (perhaps 20 % for our region of interest and time of year; Gaffen and Elliott, 1993). The effective water vapor *path* for sunlight increases when clouds are present due to multiple scattering (i.e., the light encounters more water vapor than a straight-line path would suggest). To model this effect using SPCTRAL2, we increased the water vapor input by 50 % (note that this is somewhat arbitrary) for the overcast days (i.e., $1.42 + 0.5 \times 1.42 = 2.13$). To account for the influences of clouds, recommendations from previous studies (Bird et al., 1987) were followed to fractionally increase diffuse irradiance in the region $\lambda \leq 0.55$ µm by the factor $(\lambda + 0.45)^{-1.0}$ and additionally by the factor of 0.07 in the $0.50 \leq \lambda < 0.926$ µm region.

Uncorrected SPCTRAL2 results for a clear day (using default settings mentioned above) and a cloudy day (using the modifications described in this section) reasonably followed the observed

irradiance diurnal patterns (Figure 3). The SPCTRAL2's maximum solar value was similar to the measurement for the clear day, but there were biases during periods away from local noon. This general behavior was observed on all other clear days, indicating the SPCTRAL2 algorithm did not fully represent the conditions experienced at the study site. Employing the default parameter settings regardless of time-of-day also resulted in some biases. For the cloudy day, SPCTRAL2 was not able to reproduce the local changes in cloudiness during the day and generally overestimated irradiance compared to the observations made at the top of the canopy. This result was not surprising as the SPCTRAL2 algorithm is meant to be applicable to clear sky conditions. Modifications associated with water vapor path lengths due to clouds (described above) served to increase the diffuse fraction that would be expected on a cloudy day, but had little effect on the total (direct + diffuse) irradiance. However, after applying the two corrections outlined above (see Equations 16), the total (direct + diffuse) irradiances in both PAR and total solar regions were consistent with the observations, even for the cloudy day.

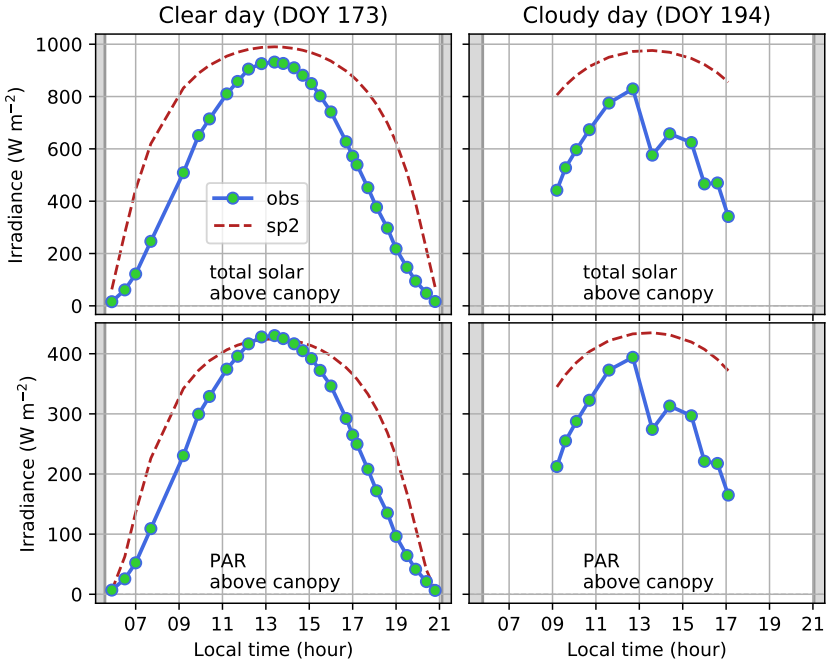

Figure 3: Measured and modeled (SPCTRAL2) total downward solar irradiance and PAR above the canopy before applying measurement-based corrections to the SPCTRAL2 spectra. Grey bars denote Sun below horizon (around sunrise or sunset).

2.5. Calculating actinic flux from irradiance quantities

The spectral actinic irradiance flux density, F_λ, generally termed "actinic flux," is the spherically integrated spectral radiance $R(\lambda, \theta, \phi)$, where θ and ϕ are the polar and azimuth angles, respectively. In contrast, the spectral irradiance, E_λ, expresses the energy spectrum impinging on a horizontal surface. As such, this quantity is measured by flat-plate radiometers (e.g., Chandrasekhar, 1960; Liou, 2002; Bohren and Clothiaux, 2006).

$$F_\lambda = \int_\phi \int_\theta R(\lambda, \theta, \phi) \sin\theta \, \mathrm{d}\theta \, \mathrm{d}\phi \tag{17}$$

$$E_\lambda = \int_\phi \int_\theta R(\lambda, \theta, \phi) \cos\theta \sin\theta \, \mathrm{d}\theta \, \mathrm{d}\phi. \tag{18}$$

Thus, the actinic flux is an expression of the amount of light available to molecules at a point in space (i.e., a very small volume) as a function of wavelength. It is usually expressed in the units photons $\mathrm{cm}^{-2}\,\mathrm{s}^{-1}\,\mathrm{nm}^{-1}$ for the distribution, or photons $\mathrm{cm}^{-2}\,\mathrm{s}^{-1}$ for the value within a wavelength band ($\mathrm{d}\lambda$). The actinic flux is the relevant quantity for the computation of photolysis rate coefficients (J values), which depend on how many photons of light molecules absorb (absorption cross-section, $\sigma(\lambda)$), how likely they undergo cleavage after absorbing (photolysis quantum yield, $\phi(\lambda)$), and the amount of available light (actinic flux $F_\lambda \equiv F(\lambda)$) (e.g., Madronich, 1987; Madronich and Flocke, 1999):

$$J = \int_\lambda \sigma(\lambda)\, \phi(\lambda)\, F(\lambda) \, \mathrm{d}\lambda. \tag{19}$$

From Eqs. 17 and 18 it is possible to discern that converting from irradiance (the quantity that is modeled in all of the radiative transfer methods) to actinic flux is nontrivial as it requires knowledge of how light is distributed among directions (Kylling et al., 2003; Weele et al., 1995). Madronich (1987) demonstrated that under the assumption of isotropy for the diffuse light (reasonable in the lower atmosphere, and a requisite assumption for the streams in deriving the aforementioned methods), there are simple relationships between actinic flux and irradiance:

$$\begin{aligned} F &= \text{diffuse contribution} + \text{direct contribution} \\ &= \left(2\, E_\downarrow^{\text{diffuse}} + 2\, E_\uparrow^{\text{diffuse}}\right) + \frac{E^{\text{direct}}}{\cos\psi} \end{aligned} \tag{20}$$

where ψ is the solar zenith angle. To apply Eq. 19, values for $\sigma(\lambda)$ and $\phi(\lambda)$ were obtained from the literature (Finlayson-Pitts and Pitts, 1999; Burkholder et al., 2015).

2.6. Photochemistry

Air chemistry data to use as model input were not available from the 1995 Borden field campaign. Therefore, version 2.0 of the 1-D Atmospheric Chemistry and Canopy Exchange Simulation

System (ACCESS) model (Saylor, 2013) was applied to examine the influences of canopy radiative transfer scheme choice on photochemical processes within and above the canopy, and the overlying atmospheric boundary layer (ABL). For the comparison between two canopy radiative transfer methods (Section 3.4), we used data obtained during 5–7 July 2014 at the Chestnut Ridge Environmental Study site, Oak Ridge, TN. The default canopy radiative transfer scheme of ACCESS v2.0 was an exponential extinction formulation based on measurements within a maize canopy (Irmak and Mutiibwa, 2008). Photolysis frequencies within the canopy were computed using the relative PAR profile,

$$J_\chi(z) = \frac{I_{PAR}(z = h_c)}{I_{PAR}(z)} J_\chi(z = h_c) \tag{21}$$

where J_χ at h_c was computed from a polynomial fit to total UV (Madronich and Flocke, 1997) runs for different solar zenith angles and heights for clear-sky conditions. The two-stream scheme described in Section 2.3.2 was added to the ACCESS model to examine the sensitivity of photochemical processes to the treatment of in-canopy radiative transfer.

3. Results and Discussion

3.1. Validation of canopy radiative transfer methods

Below-canopy total solar and PAR observations were contrasted with model results to evaluate the fidelity of each of the four radiative transfer methods (Figure 4). The clear-day case was mostly well-represented by all models (except for the maximum irradiance), with mean square errors between observations and model (Beer–Lambert, two-stream, four-stream, and light multi-scattering models) results amounting to 25.8 (5.1), 22.5 (5.2), 21.9 (5.1), and 23.3 (5.2) W m^{-2} for solar (PAR), respectively. In the cloudy case, modeled below-canopy PAR better matched the observations than total solar, yielding mean square errors (PAR (global solar irradiance)) of 3.2 (28.8), 5.6 (24.0), 2.9 (14.9), 5.1 (23.0) W m^{-2} for Beer–Lambert, two-stream, four-stream, and light multi-scattering models, respectively. The maximum observed solar irradiance value almost reached 30 % greater than results obtained with any radiative transfer model, though the rest of the diurnal cycle matched reasonably well. This result could be due to changes in clearness during the day or changes in the cloud water path for the direct beam with solar zenith angle. As confirmed by previous studies (Wang, 2003; Yuan et al., 2017), results from four-stream and two-stream models more closely matched the PAR and solar irradiance observations made above the forest floor (Figure 4).

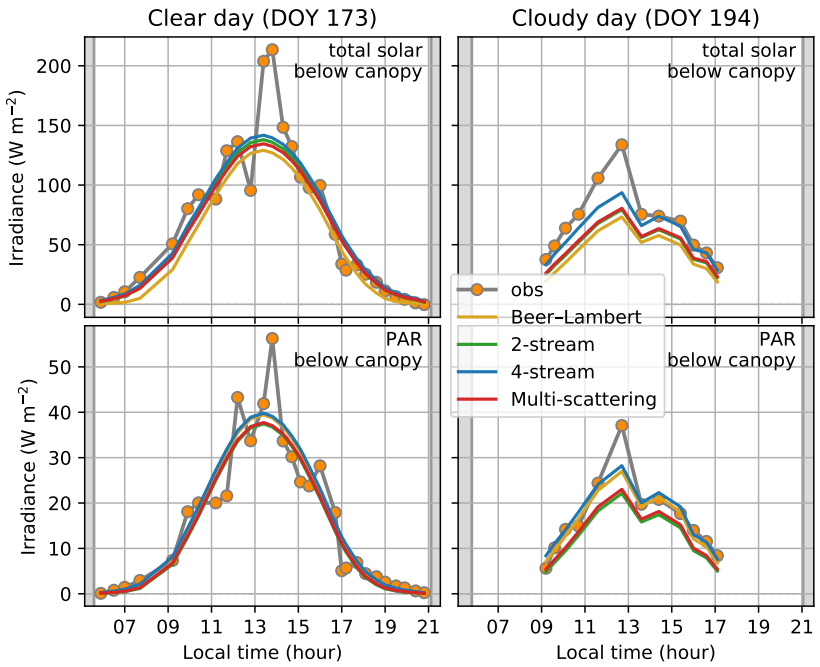

Figure 4: Measured and modeled total downward solar irradiance and PAR below the canopy. Grey bars denote Sun below horizon (around sunrise or sunset).

3.2. Comparison of canopy radiative transfer methods

Using the top-of-canopy spectra from SPCTRAL2 for the Borden forest, the disposition of in-canopy spectral irradiance was computed. For local noontime conditions (i.e., solar zenith angle 22° for day-of-year 173), the forest canopy substantially attenuated the spectral irradiance (Figure 5). The spectrum reaching the forest floor was also considerably different compared to that at the canopy top. The wavelength dependence of leaf absorption and scattering (Figure 2) resulted in shifts of the maximum irradiance towards the N-IR, primarily due to the low absorbance in the 0.8–1.2 µm region. Similar spectral irradiance profiles were estimated with the other three radiative transfer approaches (results not shown).

All of the radiative transfer models estimated similar spectral irradiance profiles in the visible waveband. In the N-IR, the Beer–Lambert approach underestimated the spectral irradiance profiles compared to the other three methods (Figure 6). Small differences (< 10 %) in the attenuation of spectral irradiance prevailed among two-stream, four-stream, and multi-scattering methods. These differences resulted because of dissimilarities in the treatment of extinction of diffuse solar irradiance and conversion of scattered direct to diffuse light; extinction of the direct solar beam is identically treated in all four models.

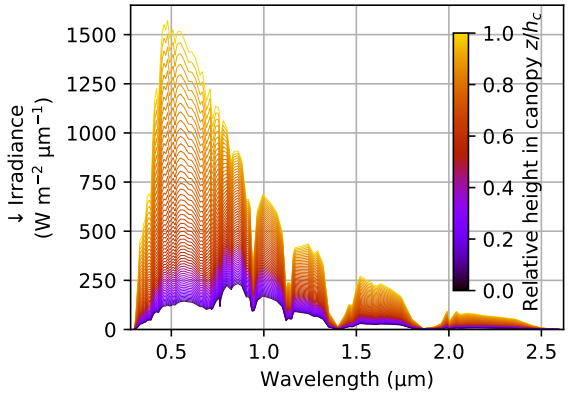

Figure 5: Spectral downward (direct+diffuse) irradiance at each level of the two-stream model for the Borden forest on day-of-year (DOY) 173 at 13:24 local time (LT; this corresponds to the measurement with the smallest solar zenith angle). Lighter colored spectra are higher in the canopy and darker are nearer to the ground. The canopy height h_c is 22 m.

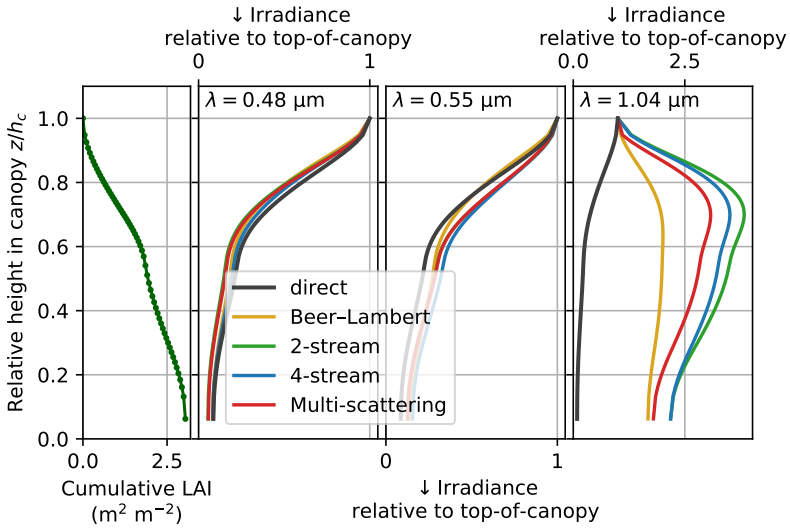

Figure 6: For the Borden forest on day-of-year (DOY) 173 at 13:24 LT. Panel 1 shows the cumulative leaf area index profile for reference, and panels 2–4 display downward solar irradiance in the model waveband closest to the indicated wavelength relative to their top-of-canopy value. Diffuse downward irradiances for each model are in color and the direct beam solution in black. Direct solar beam penetration is calculated the same way in all models (Eq. 4).

Notable differences were apparent in the estimated profiles of total solar diffuse irradiance. For example, the multi-scattering model estimated greater amounts of upward diffuse irradiance in the forest crown than the other methods. All models but the Beer–Lambert approach computed similar upward diffuse irradiance in the lower canopy depths ($z/h_c > 0.75$). Compared to the other methods, the Beer–Lambert approach consistently underestimated the downward diffuse irradiance

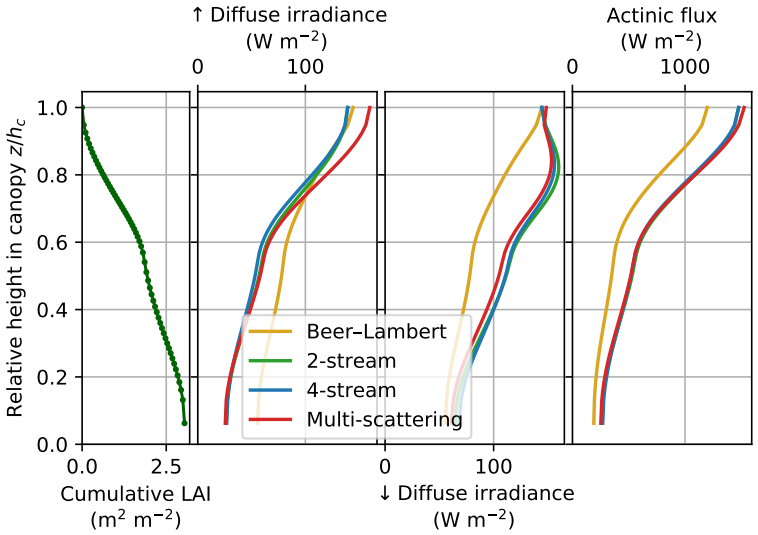

Figure 7: For the Borden forest on day-of-year (DOY) 173 at 13:24 LT. Values in panels 2–4 are integrated over all wavelengths. Panel 1 shows the cumulative leaf area index profile for reference.

with canopy depth (Figure 7). One unique result obtained with two-stream, four-stream, and multi-scattering models was the enhanced downward diffuse irradiance in the upper canopy, culminating in the maximum at $z/h_c = 0.8$. This enhancement of downward diffuse with respect to the top-of-canopy value was in response to light scattering by the abundance of foliage elements in the forest crown. The total solar actinic flux profiles as per calculations using Eq. 20 were almost identical for the two-stream, four-stream, and multi-scattering methods (Figure 7). Given the small solar zenith angle and the choice of isotropic leaf element scattering phase function in the four-stream formulation, it is not surprising that the four-stream results for total solar were not more different from the two-stream approach. The Beer–Lambert model produced significantly different actinic flux because it did not explicitly consider upward diffuse, unlike the other models, even with the Eq. 7 correction. This result was consistent with previous findings (Wang, 2003), which indicated that the Beer–Lambert approach underestimated the disposition of irradiance in the canopy compared to the four-stream method.

The differences in actinic flux among the four models changed with solar zenith angle and exhibited marked wavelength dependence (Figure 8). With respect to the two-stream, spectral actinic flux anomalies exceeded ± 100 W m^{-2} µm^{-1} ($\sim 10\%$) in some cases. For the Beer–Lambert approach, the anomaly dependence on wavelength did not change much with solar zenith angle. Four-stream and multi-scattering models revealed evident regime shifts at high solar zenith angle in the N-IR and varied from positive to negative anomalies with respect to the two-stream method.

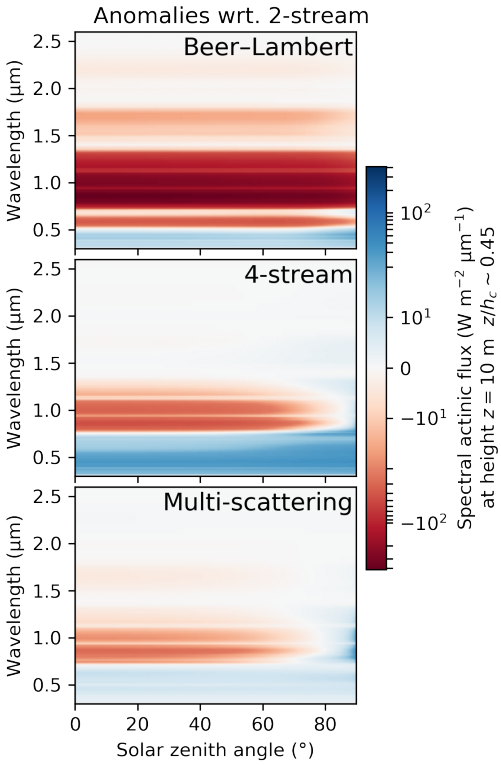

Figure 8: Dependence on (or sensitivity to) solar zenith angle of the distribution of actinic flux among schemes. Mid-canopy spectral actinic flux for the two-stream scheme is compared to that for the other three schemes. SPCTRAL2 output for the Borden forest day-of-year (DOY) 173 at 13:24 local time (LT; closest to local Solar noon) is used as the top-of-canopy boundary condition (i.e., only the solar zenith angel is changed and actual solar zenith angle is approximately 21°).

This result occurred because these two methods better accounted for radiative transfer at solar zenith angles approaching 90°.

3.3. In-canopy photolysis frequency calculations

For the most common molecules amenable to undergo photochemical reactions in the atmospheric boundary layer, the photolysis frequencies (calculated using Eq. 19) decreased with canopy depth in response to modifications of wavelengths (Figure 5) and attenuation of actinic irradiance (Figure 7). For the case of NO_2 at 13:24 hours (local time) during day of the year (DOY) 173 (Figure 9), the calculated photolysis frequencies varied from $1 \times 10^{-3}\,\mathrm{s}^{-1}$ in the middle of the canopy to $8 \times 10^{-3}\,\mathrm{s}^{-1}$ above the canopy. Such photolysis frequencies nearly matched field observations made in mid-latitude regions (Bohn, 2006). The Beer–Lambert method underestimated the photolysis frequencies in the upper ($\frac{z}{h_c} > 0.7$) canopy compared to the other three models. Within the crown of the forest ($z/h_c > 0.9$), all models computed similar photolysis frequencies and nearly

matched the values obtained with the PAR weighting method (i.e., Eq. 21). However, in the lower region of the canopy, marked differences in the NO_2 photolysis frequencies prevailed, with differences between PAR weighting method and spectral models exceeding 20 %. In the lower canopy, two-stream and multi-scattering spectral models computed photolysis frequencies that exceeded 50 % of the ones determined with the PAR weighting method. The percent error profile from the four-stream model closely followed the Beer–Lambert rather than the two-stream. The two-stream and multi-scattering models consistently gave greater (more positive) photolysis frequency errors than the other two models. Similar profiles in photolysis frequencies were estimated for O_3 (data not shown).

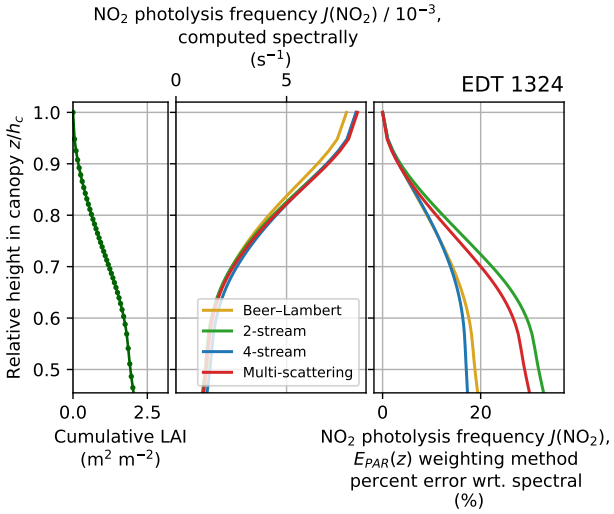

Figure 9: The NO_2 photolysis frequency profiles for Borden DOY 173, 1995 (panel 2), and comparisons between the spectral (technically, multi-band) calculation and the PAR weighting method (panel 3). Percent error for the PAR weighting method is computed using the spectral calculation as the reference: (PAR-weighting − spectral)/spectral×100. Only data for the the upper region of the canopy are shown.

For each radiative transfer model, the in-canopy integrated average photolysis frequency (i.e., $\frac{1}{h_c}\int_0^{h_c} J(z)\,\mathrm{d}z$) was calculated and results were contrasted with the ones obtained with the PAR weighting method (i.e., Eq. 21). In the case of the sample molecule NO_2 (Figure 10), a diurnal pattern emerged in the percent differences between the four models and the PAR weighting method, with differences ranging from 0 to 12 % during 8 to 18 hours (local time). These results indicated that the PAR weighting method overestimated in-canopy photolysis frequency, and maximum discrepancies of 12 % were estimated during local solar noon. All radiative transfer models properly accounted for the temporal pattern of NO_2 photolysis. However, as solar zenith angles increased

and attained high values ($\geq 80°$) close to sunrise and sunset, the percent errors became negative in response to the exponential increases in direct solar beam path length for the assumed horizontally homogeneous semi-infinite canopy. The longer path lengths for the direct solar beam through the canopy at high solar zenith angles increased absorption within a given model layer and likely resulted in greater frequency of multiple light scattering within leaf layers. Path lengths from the Sun through the atmosphere were also longer, leading to greater amounts of diffuse light in the top-of-canopy downwelling irradiance. When combined, these two factors contributed to greater differences among models during time periods close to sunrise and sunset. During the middle of the day, the greatest differences in photolysis frequency were computed for the two-stream model, followed by multi-scattering, Beer-Lambert, and four-stream methods (Figure 10). Extinction coefficients (computed as $-\log\left(I_{\text{below}}/I_{h_c}\right) L_{\text{tot}}$) for UV actinic flux and irradiance in the PAR range (Figure 10) partly explained the temporal variability in the computed in-canopy photolysis frequency error. During the period 8 to 18 hours, the relative attenuation for UV actinic flux was greater than that for irradiance in the PAR region, but the opposite occurred close to sunrise and sunset. The time at which the PAR extinction coefficient became greater than that for UV actinic flux was near to that when the percent error from the PAR weighting method reached negative values.

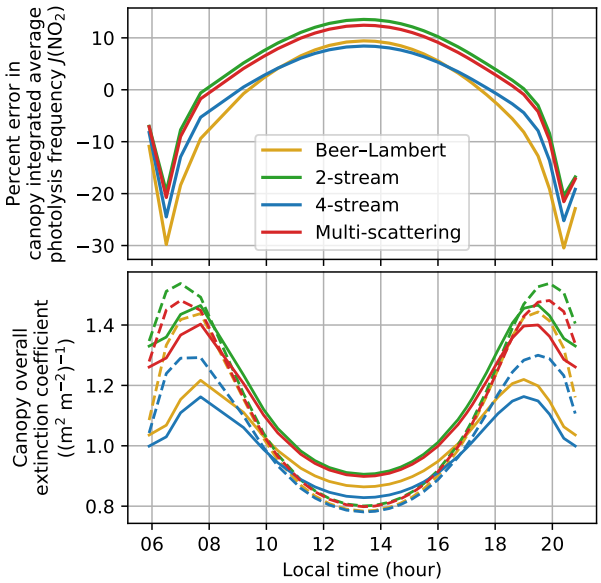

Figure 10: Upper panel: percent error in canopy integrated average NO_2 photolysis frequency for the PAR weighting method. Canopy integrated average photolysis is calculated as $1/h_c \int_0^{h_c} J(z)\,\mathrm{d}z$. The absolute errors were highest around local Solar noon, when the photolysis frequencies themselves were largest. Lower panel: modeled canopy overall extinction coefficient for UV actinic flux (solid) and irradiance in the PAR range (dashed).

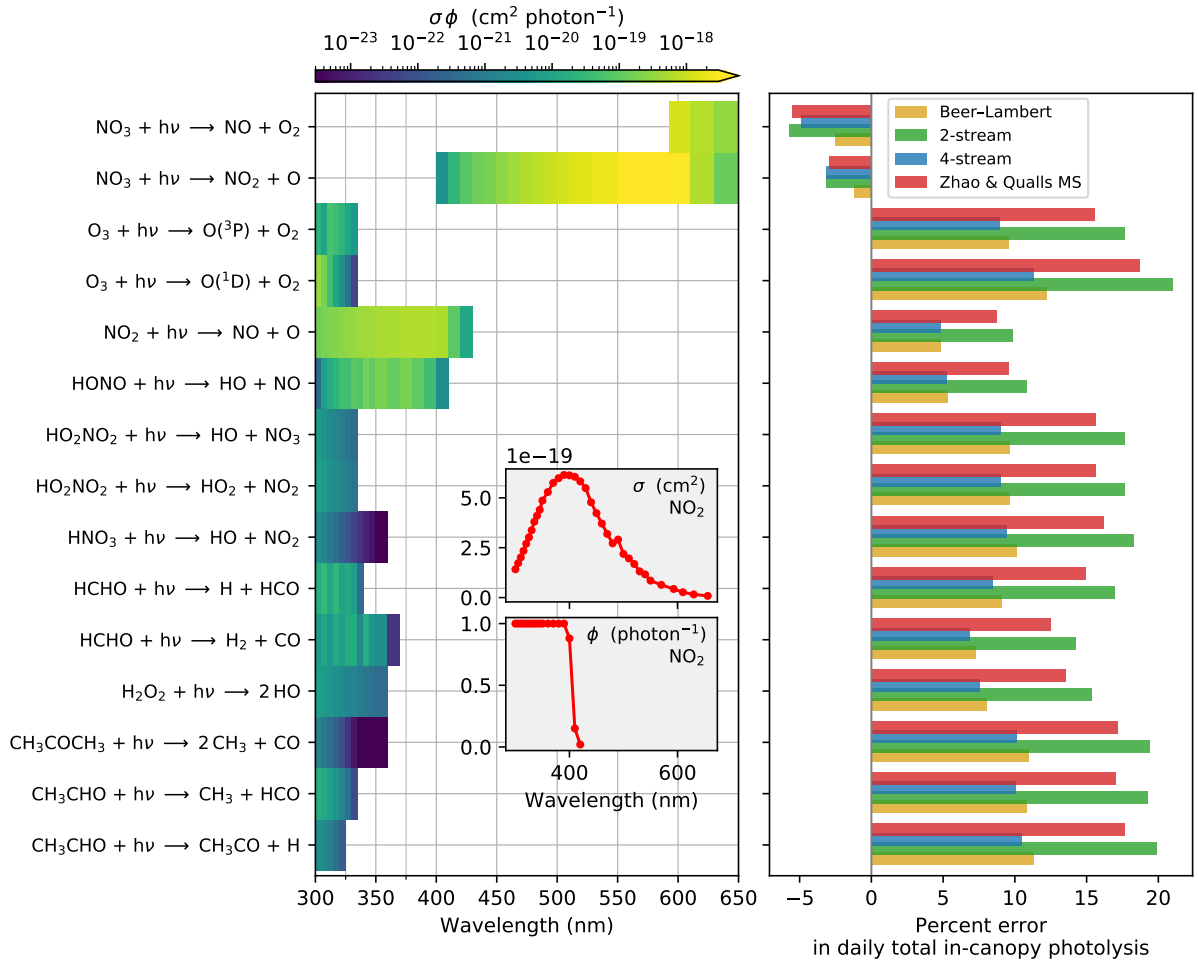

Figure 11: For the Borden forest on day-of-year (DOY) 173. Left: the product of the absorption cross-section $\sigma(\lambda)$ (cm^2) and photolysis quantum yield $\phi(\lambda)$ (photon^{-1}) for sample molecules amenable to photolysis. The inset provides the spectral $\sigma(\lambda)$ and $\phi(\lambda)$ for a sample molecule, NO_2. Right: percent error in daily total canopy integrated photolysis frequency for the PAR weighting method compared to the spectral calculation. The PAR weighting and spectral results were computed on a method-by-method basis.

In-canopy integrated average photolysis frequencies also varied depending on actinic light wavelengths and chemical species. On a daily basis, when the four radiative transfer models were contrasted with the PAR weighting method, results indicated that molecules undergoing photolysis in the shortest light wavelengths appeared to have the largest discrepancies. Examples of such molecules were O_3, peroxynitric acid (HO_2NO_2), HNO_3, HCHO, CH_3CHO, and CH_3COCH_3 whose differences amounted to 10–20 % (Figure 11). In addition, error relationships among the radiative transfer models indicated consistent results among the different photochemical reactions, with the two-stream model yielding the highest PAR weighting error and the four-stream model exhibiting

the lowest error (except for the two negative cases). For NO_3, which undergoes photolysis even up to the N-IR (Figure 11), the PAR weighting method overestimated photolysis frequency and the errors for the three more complex models were very similar. In general, the greater relative attenuation of UV actinic flux compared to irradiance in the PAR range (Figure 10) can explain the PAR weighting method's overestimation to a large extent. This distinction was most prominent in the two-stream and multi-scattering models and less so in the Beer–Lambert and four-stream models.

3.4. Canopy model simulations

Photochemical simulations were performed with the 1-D canopy-chemistry model ACCESS to evaluate the impacts that different photolysis rates, due to differences in canopy radiative transfer methods, can have on the chemistry and associated turbulent transport of gases from the canopy to the overlying ABL. Based on the results of Figure 11 and relevance of plant-emitted gases, the focus of the evaluation was on chemical species such as O_3, NO_3, NO_2, HCHO, HO, NO_3, and isoprene (C_5H_8; Figure 12). As noted above (Figure 3), the two-stream model closely matched the disposition of sunlight in the Borden forest canopy and is included in climate models (e.g., Yuan et al., 2017). Therefore, sample photochemical simulations (Figure 12) were computed using the two-stream method and contrasted with a control simulation using the scheme originally included in ACCESS (Irmak and Mutiibwa, 2008). For the chemical species whose net destruction primarily depended on photolytic reactions (e.g., O_3, NO_3, NO_2), the two-stream radiative transfer gave higher gas concentrations within the canopy in response to the lower simulated actinic light reaching the lower depths of the canopy. In contrast, simulated isoprene profiles using the two-stream model stayed substantially lower (64 %) compared to the control. The HCHO profiles (Figure 12) followed similar patterns as C_5H_8 oxidation was the major source of HCHO. Isoprene emission depends on PAR levels as well as light quality, temperature, and stresses imposed by processes such as droughts (Fuentes et al., 2000).

Additional experiments using the two-stream scheme for either in-canopy photolysis or the visible light profile (PPFD: photosynthetic photon flux density, used to derive emissions) allow us to attribute the differences. For isoprene, emissions differences explain about 98 % of the differences in isoprene mixing ratio. Using the two-stream approach for in-canopy photolysis only, isoprene levels are slightly higher (3.6 %), due to lower light levels and consequent reduced formation of HO. When using the two-stream method only for PPFD, however, the mean isoprene profile is nearly

identical to that for the full two-stream simulation. The HO presented the only case where the two-stream and control profiles crossed, around $\frac{z}{h_c} = 0.4$ (Figure 12). In the lower regions of the canopy, there was less HO formation from the O_3 photolysis pathway in the two-stream simulation because light levels were much lower. In the upper half of the canopy, light in the two-stream simulation was enough to promote HO formation, but the lower isoprene emissions resulted in a smaller HO sink (due to the reaction $C_5H_8 + HO \longrightarrow$ Products) and reduced monoterpene emissions provided less an of ozone sink (allowing for greater HO formation). The f_j-only and PPFD-only results confirm this interpretation, demonstrating that there are two HO regimes in the canopy for the full two-stream simulation: emissions-driven in the upper canopy (reduced monoterpene levels giving a smaller O_3 sink), and light-driven in the lower canopy (photolysis frequency). Both of these are aspects of the photo-production of HO from O_3 (Equations 1 and 3).

4. Summary and Conclusions

Utilizing radiation measurements above and below a deciduous forest, a new approach was developed and evaluated to investigate broadband irradiance and spectral actinic flux as a function of canopy depth. Four radiative transfer models were also appraised to determine the disposition of solar irradiance within the forest. Broadband solar irradiance was converted to spectral irradiance and canopy radiative transfer was computed based on the wavelength-dependent radiative properties of the foliage. The Beer–Lambert model notably underestimated total solar irradiance and actinic flux in the mid and upper regions of the canopy whereas the two-stream, four-stream, and light multi-scattering methods provided consistently similar results. In part, the underperformance of the Beer–Lambert model owed to unaccounted-for light scattering occurring among the considered leaf layers. Compared to broadband solar irradiance measurements made above the forest floor and for solar zenith angles $\leq 80°$, model (Beer–Lambert, two-stream, four-stream, and light multi-scattering) results differed by 22 (11), 19 (19), 12 (10), and 18 % (17 %) during cloudy (clear) conditions, respectively. Therefore, we conclude that two-stream and four-stream models are the most reliable (yet simple) approaches to investigate photochemical reactions in plant canopies.

Two-stream, four-stream, and light multi-scattering methods estimated similar actinic flux profiles. Compared to these, the Beer–Lambert model consistently underestimated the disposition of actinic irradiance within the canopy. Modeled spectral actinic flux profiles allowed for direct photolysis frequency calculations as a function of canopy depth to compare with the ones obtained with the commonly employed PAR weighting method. Compared to calculations of photolysis

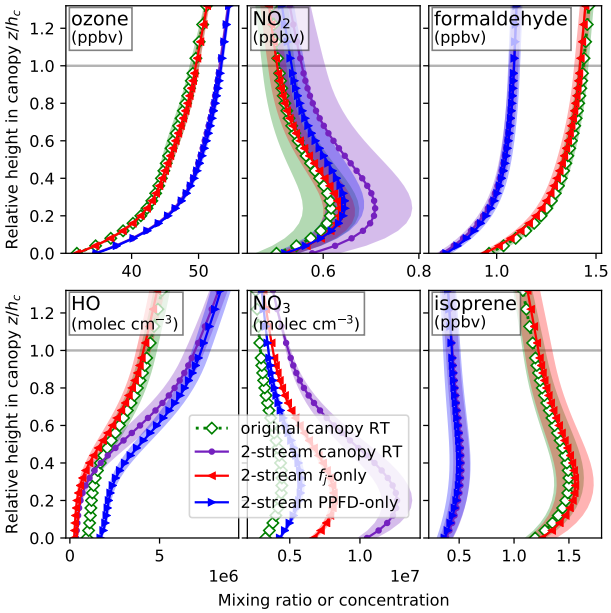

Figure 12: During 10:00–14:00 hours, average profiles of mixing ratio or concentration for several species were computed. The ACCESS simulation of the Chestnut Ridge canopy (Chestnut Ridge Environmental Study site, located on the US Department of Energy reservation near Oak Ridge National Lab) during 5–7 July 2014 (data came from NOAA Air Resources Laboratory, Atmospheric Turbulence Diffusion Division). The shading shows the standard deviation during the averaging period (9 profiles). A version of the model using a two-stream radiative transfer approach in the canopy (purple) is compared to the standard model configuration (green), which uses a simpler canopy radiative transfer scheme. In the ACCESS model the canopy radiative transfer solutions are used for two things: the profile of photolysis weighting factors ($f_j(z)$) and the PPFD profile (photosynthetic photon flux density; used by the emissions parameterizations). Red indicates an experiment with the two-stream scheme only used for f_j and blue an experiment with the two-stream only used for the PPFD profile. The markers indicate model levels.

frequency from spectral actinic flux using the four radiative transfer models, the PAR weighting method over-predicted the daily integrated in-canopy photolysis frequency of all studied molecules but NO_3. The errors were largest for molecules such as O_3 and CH_3CHO, reaching 20 % for calculations with the two-stream model. Consequently, we conclude and recommend to employ an explicitly defined spectral radiative transfer model using a scheme such as the four-stream method to investigate photochemical processes in plant canopies.

Major differences were computed for in-canopy chemical reactions determined with a 1-D photochemical model that incorporated a detailed chemical mechanism and the two-stream model or a simple exponential formulation with canopy radiative transfer. For canopy integrated concentrations in the two-stream simulation, gas concentration differences ranged from 8 % for O_3 to 77 %

for NO_3 compared to those estimated with the original scheme. In the case of HCHO and C_5H_8 computed with the original scheme, gas concentrations were 24 % and 64 % lower than values computed using the two-stream model. The principal reason for the discrepancies in these two gases is that the original scheme over-predicted light levels in the lower canopy, resulting in larger isoprene emission rates. Additionally, the higher light levels in the original scheme experiment promoted increased photolysis, especially in the lower canopy. This was more important for gases whose levels are more light-dependent, like HO and NO_3. In summary, this study concludes that accurate and spectrally resolved canopy radiative transfer models are critically necessary to realistically determine chemical reactions and gas concentrations within plant canopies and in the immediately overlying atmospheric boundary layer.

5. Acknowledgments

Z. Moon acknowledges support from the NCAS-M (NOAA (National Oceanic and Atmospheric Administration) Center for Atmospheric Sciences and Meteorology), Educational Partnership Program, U.S. Department of Commerce, under Agreement No. NA16SEC4810006-NCAS-M. We thank the Editor for timely processing of the article. Also, we thank two anonymous reviewers who provided excellent comments to improve the article.

References

Aschmann, S.M., Arey, J., Atkinson, R., 2002. OH radical formation from the gas-phase reactions of O_3 with a series of terpenes. Atmospheric Environment 36, 4347–4355. doi:10.1016/S1352-2310(02)00355-2.

Ashworth, K., Chung, S.H., Griffin, R.J., Chen, J., Forkel, R., Bryan, A.M., Steiner, A.L., 2015. FORest Canopy Atmosphere Transfer (FORCAsT) 1.0: A 1-D model of biosphere–atmosphere chemical exchange. Geosci. Model Dev. 8, 3765–3784. doi:10.5194/gmd-8-3765-2015.

Atkinson, R., 2000. Atmospheric chemistry of VOCs and NO_x. Atmospheric Environment 34, 2063–2101. doi:10.1016/S1352-2310(99)00460-4.

Baldocchi, D.D., Matt, D.R., Hutchison, B.A., McMillen, R.T., 1984. Solar radiation within an oak—hickory forest: An evaluation of the extinction coefficients for several radiation components during fully-leafed and leafless periods. Agricultural and Forest Meteorology 32, 307–322. doi:10.1016/0168-1923(84)90056-X.

Barthelmie, R.J., Pryor, S.C., 1999. A model mechanism to describe oxidation of monoterpenes leading to secondary organic aerosol: 1. α-pinene and β-pinene. Journal of Geophysical Research: Atmospheres 104, 23657–23699. doi:10.1029/1999JD900382.

Bird, R.E., 1984. A simple, solar spectral model for direct-normal and diffuse horizontal irradiance. Solar Energy 32, 461–471. doi:10.1016/0038-092X(84)90260-3.

Bird, R.E., Riordan, C., 1986. Simple Solar Spectral Model for Direct and Diffuse Irradiance on Horizontal and Tilted Planes at the Earth's Surface for Cloudless Atmospheres. Journal of Climate and Applied Meteorology 25, 87–97. doi:10.1175/1520-0450(1986)025<0087:SSSMFD>2.0.CO;2.

Bird, R.E., Riordan, C.J., Myers, D.R., 1987. Investigation of a Cloud-Cover Modification to SPCTRAL2, SERI's Simple Model for Cloudless-Sky, Spectral Solar Irradiance. Technical Report SERI/TR-215-3038. Solar Energy Research Inst., Golden, CO (USA). doi:10.2172/6436871.

Bohn, B., 2006. Solar spectral actinic flux and photolysis frequency measurements in a deciduous forest. Journal of Geophysical Research: Atmospheres 111, D15303. doi:10.1029/2005JD006902.

Bohn, B., Corlett, G.K., Gillmann, M., Sanghavi, S., Stange, G., Tensing, E., Vrekoussis, M., Bloss, W.J., Clapp, L.J., Kortner, M., Dorn, H.P., Monks, P.S., Platt, U., Plass-Dülmer, C., Mihalopoulos, N., Heard, D.E., Clemitshaw, K.C., Meixner, F.X., Prevot, A.S.H., Schmitt, R., 2008. Photolysis frequency measurement techniques: Results of a comparison within the ACCENT project. Atmos. Chem. Phys. 8, 5373–5391. doi:10.5194/acp-8-5373-2008.

Bohren, C.F., Clothiaux, E.E., 2006. Fundamentals of Atmospheric Radiation - An Introduction with 400 Problems. Wiley-VCH.

Burkholder, J.B., Sander, S.P., Abbatt, J.P.D., Barker, J.R., Huie, R.E., Kolb, C.E., Kurylo, M.J., Orkin, V.L., Wilmouth, D.M., Wine, P.H., 2015. Chemical Kinetics and Photochemical Data for Use in Atmospheric Studies: Evaluation Number 18. Technical Report. Pasadena, CA : Jet Propulsion Laboratory, National Aeronautics and Space Administration, 2015.

Campbell, G.S., Norman, J.M., 2012. An Introduction to Environmental Biophysics. 2 ed., Springer Science & Business Media, New York.

Carlton, A.G., Wiedinmyer, C., Kroll, J.H., 2009. A review of Secondary Organic Aerosol (SOA) formation from isoprene. Atmos. Chem. Phys. 9, 4987–5005. doi:10.5194/acp-9-4987-2009.

Chandrasekhar, S., 1960. Radiative Transfer. Dover, New York.

Dickinson, R.E., 1983. Land Surface Processes and Climate—Surface Albedos and Energy Balance. Advances in Geophysics 25, 305–353. doi:10.1016/S0065-2687(08)60176-4.

Doughty, D., 2014. Particulate Matter and Trace-Gas Changes at Beltsville, MD, and Influences on Cloud Condensation Nuclei. PhD Dissertation. Penn State. University Park, PA.

Finlayson-Pitts, B.J., Pitts, Jr., J.N., 1999. Chemistry of the Upper and Lower Atmosphere: Theory, Experiments, and Applications. Academic Press.

Forkel, R., Klemm, O., Graus, M., Rappenglück, B., Stockwell, W.R., Grabmer, W., Held, A., Hansel, A., Steinbrecher, R., 2006. Trace gas exchange and gas phase chemistry in a Norway spruce forest: A study with a coupled 1-dimensional canopy atmospheric chemistry emission model. Atmospheric Environment 40, 28–42. doi:10.1016/j.atmosenv.2005.11.070.

Fuentes, J.D., Chamecki, M., Nascimento dos Santos, R.M., Von Randow, C., Stoy, P.C., Katul, G., Fitzjarrald, D., Manzi, A., Gerken, T., Trowbridge, A., Souza Freire, L., Ruiz-Plancarte, J., Fur-

tunato Maia, J.M., Tóta, J., Dias, N., Fisch, G., Schumacher, C., Acevedo, O., Rezende Mercer, J., Yañez-Serrano, A.M., 2016. Linking Meteorology, Turbulence, and Air Chemistry in the Amazon Rain Forest. Bull. Amer. Meteor. Soc. 97, 2329–2342. doi:10.1175/BAMS-D-15-00152.1.

Fuentes, J.D., Gu, L., Lerdau, M., Atkinson, R., Baldocchi, D., Bottenheim, J.W., Ciccioli, P., Lamb, B., Geron, C., Guenther, A., Sharkey, T.D., Stockwell, W., 2000. Biogenic Hydrocarbons in the Atmospheric Boundary Layer: A Review. Bull. Amer. Meteor. Soc. 81, 1537–1575. doi:10.1175/1520-0477(2000)081<1537:BHITAB>2.3.CO;2.

Fuentes, J.D., Wang, D., Bowling, D.R., Potosnak, M., Monson, R.K., Goliff, W.S., Stockwell, W.R., 2007. Biogenic Hydrocarbon Chemistry within and Above a Mixed Deciduous Forest. Journal of Atmospheric Chemistry 56, 165–185. doi:10.1007/s10874-006-9048-4.

Gaffen, D.J., Elliott, W.P., 1993. Column Water Vapor Content in Clear and Cloudy Skies. Journal of Climate 6, 2278–2287. doi:10.1175/1520-0442(1993)006<2278:CWVCIC>2.0.CO;2.

Gerken, T., Chamecki, M., Fuentes, J.D., 2017. Air-Parcel Residence Times Within Forest Canopies. Boundary-Layer Meteorol 165, 29–54. doi:10.1007/s10546-017-0269-7.

Goudriaan, J., 1977. Crop Micrometeorology : A Simulation Study. Phd. Pudoc. Wageningen.

Guenther, A.B., Jiang, X., Heald, C.L., Sakulyanontvittaya, T., Duhl, T., Emmons, L.K., Wang, X., 2012. The Model of Emissions of Gases and Aerosols from Nature version 2.1 (MEGAN2.1): An extended and updated framework for modeling biogenic emissions. Geosci. Model Dev. 5, 1471–1492. doi:10.5194/gmd-5-1471-2012.

Irmak, S., Mutiibwa, D., 2008. Dynamics of Photosynthetic Photon Flux Density and Light Extinction Coefficient to Assess Radiant Energy Interactions for Maize Canopy. Transactions of the ASABE 51, 1663–1673. doi:10.13031/2013.25323.

Kroll, J.H., Seinfeld, J.H., 2008. Chemistry of secondary organic aerosol: Formation and evolution of low-volatility organics in the atmosphere. Atmospheric Environment 42, 3593–3624. doi:10.1016/j.atmosenv.2008.01.003.

Kuusk, A., 2018. 3.03 - Canopy Radiative Transfer Modeling, in: Liang, S. (Ed.), Comprehensive Remote Sensing. Elsevier, Oxford, pp. 9–22. doi:10.1016/B978-0-12-409548-9.10534-2.

Kylling, A., Webb, A.R., Bais, A.F., Blumthaler, M., Schmitt, R., Thiel, S., Kazantzidis, A., Kift, R., Misslbeck, M., Schallhart, B., Schreder, J., Topaloglou, C., Kazadzis, S., Rimmer, J., 2003. Actinic flux determination from measurements of irradiance. Journal of Geophysical Research: Atmospheres 108, 4506. doi:10.1029/2002JD003236.

Li, J., Dobbie, J.S., 1998. Four-Stream Isosector Approximation for Solar Radiative Transfer. Journal of the Atmospheric Sciences 55, 558–567. doi:10.1175/1520-0469(1998)055<0558:FSIAFS>2.0.CO;2.

Liou, K.N., 2002. An Introduction to Atmospheric Radiation. volume 84 of *International Geophysics*. 2 ed., Academic Press.

Madronich, S., 1987. Photodissociation in the atmosphere: 1. Actinic flux and the effects of ground reflections and clouds. Journal of Geophysical Research: Atmospheres 92, 9740–9752. doi:10.1029/JD092iD08p09740.

Madronich, S., Flocke, S., 1997. Theoretical Estimation of Biologically Effective UV Radiation at the Earth's Surface, in: Zerefos, C.S., Bais, A.F. (Eds.), Solar Ultraviolet Radiation, Springer Berlin Heidelberg. pp. 23–48.

Madronich, S., Flocke, S., 1999. The Role of Solar Radiation in Atmospheric Chemistry, in: Boule, D.P. (Ed.), Environmental Photochemistry. Springer Berlin Heidelberg. number 2 / 2L in The Handbook of Environmental Chemistry, pp. 1–26. doi:10.1007/978-3-540-69044-3_1.

Makar, P.A., Fuentes, J.D., Wang, D., Staebler, R.M., Wiebe, H.A., 1999. Chemical processing of biogenic hydrocarbons within and above a temperate deciduous forest. Journal of Geophysical Research: Atmospheres (1984–2012) 104, 3581–3603. doi:10.1029/1998JD100065.

Millet, D.B., Jacob, D.J., Turquety, S., Hudman, R.C., Wu, S., Fried, A., Walega, J., Heikes, B.G., Blake, D.R., Singh, H.B., Anderson, B.E., Clarke, A.D., 2018. Formaldehyde distribution over North America: Implications for satellite retrievals of formaldehyde columns and isoprene emission. Journal of Geophysical Research: Atmospheres doi:10.1029/2005JD006853.

Monteith, J.L., Unsworth, M.H., 2013. Principles of Environmental Physics: Plants, Animals, and the Atmosphere. 4 ed., Academic Press, Oxford.

Myneni, R.B., Asrar, G., Kanemasu, E.T., 1987. Light scattering in plant canopies: The method of Successive Orders of Scattering Approximations (SOSA). Agricultural and Forest Meteorology 39, 1–12. doi:10.1016/0168-1923(87)90011-6.

O'Halloran, T.L., Fuentes, J.D., Collins, D.R., Cleveland, M.J., Keene, W.C., 2009. Influence of air mass source region on nanoparticle events and hygroscopicity in central Virginia, U.S. Atmospheric Environment 43, 3586–3595. doi:10.1016/j.atmosenv.2009.03.033.

Palmer, P.I., Jacob, D.J., Fiore, A.M., Martin, R.V., Chance, K., Kurosu, T.P., 2003. Mapping isoprene emissions over North America using formaldehyde column observations from space. Journal of Geophysical Research: Atmospheres 108. doi:10.1029/2002JD002153.

Pandis, S.N., Paulson, S.E., Seinfeld, J.H., Flagan, R.C., 1991. Aerosol formation in the photooxidation of isoprene and β-pinene. Atmospheric Environment. Part A. General Topics 25, 997–1008. doi:10.1016/0960-1686(91)90141-S.

Paulson, S.E., Orlando, J.J., 1996. The reactions of ozone with alkenes: An important source of HO_x in the boundary layer. Geophysical Research Letters 23, 3727–3730. doi:10.1029/96GL03477.

Rinne, J., Markkanen, T., Ruuskanen, T., Petäjä, T., Keronen, P., Tang, M., Crowley, J., Rannik, Ü., Vesala, T., 2012. Effect of chemical degradation on fluxes of reactive compounds–a study with a stochastic lagrangian transport model. Atmospheric chemistry and physics 12, 4843–4854.

Saylor, R.D., 2013. The Atmospheric Chemistry and Canopy Exchange Simulation System (ACCESS): Model description and application to a temperate deciduous forest canopy. Atmos. Chem. Phys. 13, 693–715. doi:10.5194/acp-13-693-2013.

Sellers, P.J., 1985. Canopy reflectance, photosynthesis and transpiration. International Journal of Remote Sensing 6, 1335–1372. doi:10.1080/01431168508948283.

Staebler, R., Fuentes, J.D., Neumann, H., Chen, J., 1997. Light interception by a temperate deciduous forest, in: 9th Conference on Atmospheric Radiation, American Meteorological Society, Long Beach, CA. pp. 42–45.

Staebler, R.M., Fuentes, J.D., Lee, X., Puckett, K.J., Neumann, H.H., Deary, M.J., Arnold, J.A., 2000. Long term flux measurements at the Borden forest. CMOS Bulletin 28, 9–16.

694 Strong, C., Fuentes, J., Baldocchi, D., 2004. Reactive hydrocarbon flux footprints during canopy senescence. Agricultural and Forest Meteorology 127, 159–173.

696 Stroud, C., Makar, P., Karl, T., Guenther, A., Geron, C., Turnipseed, A., Nemitz, E., Baker, B., Potosnak, M., Fuentes, J.D., 2005. Role of canopy-scale photochemistry in modifying biogenic-
698 atmosphere exchange of reactive terpene species: Results from the CELTIC field study. Journal of Geophysical Research: Atmospheres 110, D17303. doi:10.1029/2005JD005775.

700 Teklemariam, T., Staebler, R.M., Barr, A.G., 2009. Eight years of carbon dioxide exchange above a mixed forest at Borden, Ontario. Agricultural and Forest Meteorology 149, 2040–2053. doi:10.
702 1016/j.agrformet.2009.07.011.

Tian, Y., Dickinson, R.E., Zhou, L., 2007. Four-stream isosector approximation for canopy ra-
704 diative transfer. Journal of Geophysical Research: Atmospheres 112, D04107. doi:10.1029/2006JD007545.

706 Van Heuklon, T.K., 1979. Estimating atmospheric ozone for solar radiation models. Solar Energy 22, 63–68. doi:10.1016/0038-092X(79)90060-4.

708 Wang, Y.P., 2003. A comparison of three different canopy radiation models commonly used in plant modelling. Functional Plant Biology 30, 143–152. doi:10.1071/fp02117.

710 Weele, M.V., Arellano, J.V.G.D., Kuik, F., 1995. Combined measurements of UV-A actinic flux, UV-A irradiance and global radiation in relation to photodissociation rates. Tellus B: Chemical
712 and Physical Meteorology 47, 353–364. doi:10.3402/tellusb.v47i3.16054.

Widlowski, J.L., Mio, C., Disney, M., Adams, J., Andredakis, I., Atzberger, C., Brennan, J.,
714 Busetto, L., Chelle, M., Ceccherini, G., Colombo, R., Côté, J.F., Eenmäe, A., Essery, R., Gastellu-Etchegorry, J.P., Gobron, N., Grau, E., Haverd, V., Homolová, L., Huang, H., Hunt,
716 L., Kobayashi, H., Koetz, B., Kuusk, A., Kuusk, J., Lang, M., Lewis, P.E., Lovell, J.L., Malenovský, Z., Meroni, M., Morsdorf, F., Mõttus, M., Ni-Meister, W., Pinty, B., Rautiainen, M.,
718 Schlerf, M., Somers, B., Stuckens, J., Verstraete, M.M., Yang, W., Zhao, F., Zenone, T., 2015. The fourth phase of the radiative transfer model intercomparison (RAMI) exercise: Ac-
720 tual canopy scenarios and conformity testing. Remote Sensing of Environment 169, 418–437. doi:10.1016/j.rse.2015.08.016.

Widlowski, J.L., Taberner, M., Pinty, B., Bruniquel-Pinel, V., Disney, M., Fernandes, R., Gastellu-Etchegorry, J.P., Gobron, N., Kuusk, A., Lavergne, T., Leblanc, S., Lewis, P.E., Martin, E., Mõttus, M., North, P.R.J., Qin, W., Robustelli, M., Rochdi, N., Ruiloba, R., Soler, C., Thompson, R., Verhoef, W., Verstraete, M.M., Xie, D., 2007. Third Radiation Transfer Model Intercomparison (RAMI) exercise: Documenting progress in canopy reflectance models. Journal of Geophysical Research: Atmospheres 112. doi:10.1029/2006JD007821.

Yuan, H., Dai, Y., Dickinson, R.E., Pinty, B., Shangguan, W., Zhang, S., Wang, L., Zhu, S., 2017. Reexamination and further development of two-stream canopy radiative transfer models for global land modeling. Journal of Advances in Modeling Earth Systems 9, 113–129. doi:10.1002/2016MS000773.

Zhao, W., Qualls, R.J., 2005. A multiple-layer canopy scattering model to simulate shortwave radiation distribution within a homogeneous plant canopy. Water Resources Research 41, W08409. doi:10.1029/2005WR004016.